Evolution of the crack patterns in nanostructured films with subsequent wetting and drying cycles

David McIlroy[1] and Ludovic Pauchard[2]

[1] *Oklahoma State University - Stillwater, USA*
[2] *Université Paris-Saclay, CNRS, FAST, 91405, Orsay, France*

PACS nn.mm.xx – First pacs description
PACS nn.mm.xx – Second pacs description
PACS nn.mm.xx – Third pacs description

Abstract –Crack patterns in coatings present various morphologies as a signature of the matter to external stresses. Brittle films generally show a network of connected cracks due to a hierarchical formation process. On the contrary, non-sequential crack growth leads to a different morphology with few junctions. The present work focuses on the evolution of both crack networks under the effect of repeated stresses. The experimental work is performed through porous thin films over subsequent wetting and drying processes. The non-connected network of cracks is investigated through nanostructured films exhibiting compliant and elastic properties. Over repeated stresses, this crack network evolves until it reaches stabilization. The stabilization appears when the cracks stop growing and a shielding effect occurs. This behaviour is compared with a more classical connected network of cracks that do not evolve in the plane under the effect of repeated processes.

Introduction. – When coatings are subjected to high stresses, mechanical instabilities can occur. These singularities, such as cracks, affect the properties and the quality of the films. This is the case of dried particulate films that exhibit various morphologies. These patterns have been extensively observed in a variety of materials, such as ceramics, paints or particulate coatings where cracking results from solvent evaporation (fig. 1a&b). In the last, capillary forces produced by the surface tension of the solvent are sustained by the wet structure. The variety of crack patterns reflect the response of the structure to the mechanical stresses. In the present work, we report the evolution of crack morphologies under repeated stresses induced by wetting and drying processes. Classically brittle films form a connected network of cracks that do not evolve in the plane with subsequent stresses. In contrast, the non-sequential crack growth results in a branched network of cracks. This last evolves until stabilization. The present work points out the unusual dynamics and the physical parameters on which system stabilization depends. This is a common phenomenon in the formation of desiccation cracks on soil surfaces and craquelures in art paintings that are confronted with variations in environmental stresses throughout their lifetime [1–3].

The evolution of crack patterns is mainly investigated here in nanostructured films made of an assembly of nanosprings. Helical nanostructured coatings provide specific electrical conductivity, in photodetection applications, as biosensors, and high interface compliance [4]. Besides, the nanospring films provide a model of elastic and compliant films where minor stress is required for a considerable strain [5]. Through these properties, the nanospring films saturated with a volatile solvent have the potential to delay cracking under drying strains. The wetting and drying process results in a branched network of cracks with low connectivity as reported in fig. 1a. In addition, under the effect of repeated wetting and drying cycles, the progressive evolution of cracking in this system and the final morphology can be precisely determined. The analysis of the film evolution shows that cracks are progressively confined through their mutual interaction. These results are compared with those encountered in the classic case of dried films [6, 7] (fig. 1b).

Experimental. – The compliant film consists of an array of helical nanowires, e.g. Vertically-Aligned NanoSprings (VANS), as shown in fig. 2a. The growth of nanowires is based on Vapor-Liquid-Solid (VLS) mechanism on a Si substrate. This process uses catalytic alloy droplets at the tip of the nanowires as preferred sites for

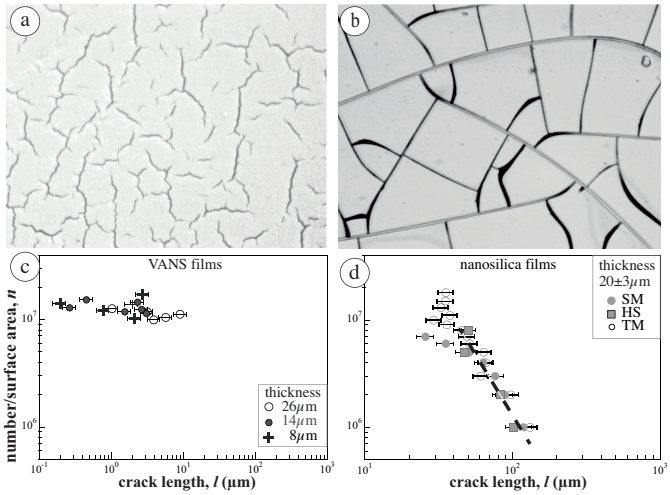

Fig. 1: Patterns of drying-induced cracks. (a) Open network of tortuous cracks in a elastic and compliant nanostructured film of springs. (b) Connection induced closed network of straight cracks of a nanosilica film (HS) characteristic of a hierarchical process. (Both films exhibit the same thickness-the image size is 100μm). (c,d) Distributions of crack lengths for the crack patterns (a) and (b), respectively (log-log scale). Measurements were performed for various film thicknesses (c) and various nanosilica films (d). The distribution of lengths follows a power law, $n \sim l^d$, characteristic of self-similar systems, with the structure remaining not dependent on scale. The dashed line indicates a fractal dimension $d = 1.8$.

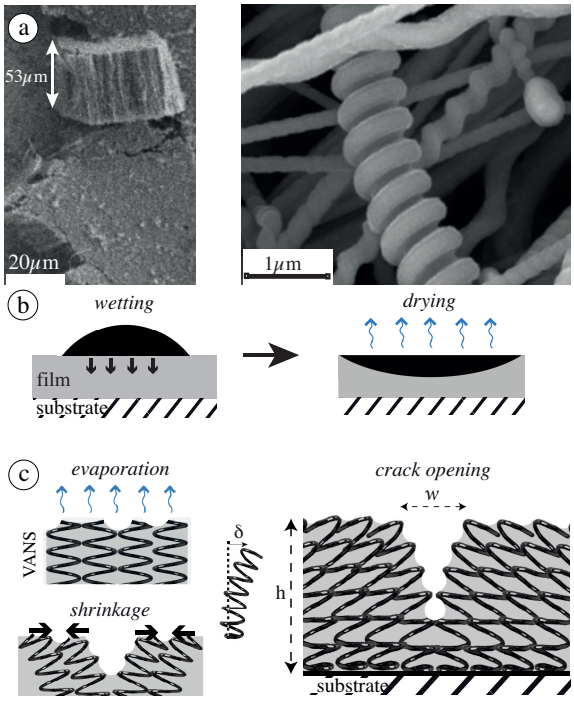

Fig. 2: (a) Scanning Electron Microscopy micrographs showing a film of aligned nanospring (left), and detail of an individual nanospring (right). (b) Illustration of the Wetting and Drying process generating stresses: deposition of a drop of a low-surface-tension liquid at the coating surface (Wetting), and drying process of the imbibed liquid in the porous coating (Drying). (c) Sketch in side view illustrating the drying shrinkage near the evaporation surface (the schematic is not to scale and gives the impression that the springs are not as long as they truly are). The nanosprings deflection, δ, results in the crack opening that is characterized by the quantity w.

deposition from the vapor. The specificity in the formation of nanospring lies in the controlled asymmetry in the contact angle at the catalytic droplet-nanowire interface. This anisotropy is responsible for a torque of the droplet [8, 9]. As a result helical structure grows perpendicularly to the substrate surface. The dense array of nanosprings is ensured by the quantity of particles sputtered onto the Si substrate and serving as the catalyst. The growth time governs the film thickness. Three film thicknesses are considered in the following: $h = 8$, 14 & 26μm. The areal density is estimated at $m = 5 \times 10^{10}$ nanosprings per cm^2 using SEM micrographs. The cohesion of the aligned nanosprings in the film ensures a structural coating. The surface energy for VANS in the air is estimated to be $\Gamma_s = 0.5 J/m^2$ provided by chemical bonding SiO_x-SiO_2, x=1-2 [10].

From a macroscopic point of view, nanospring films exhibit compliant properties. Hence, the mechanical behaviour of nanospring films was examined using nanoindentation testing. The method consists of driving a spherical tip into the sample with a controlled force as a function of the penetration depth in the material (see Supplementary Material 'S1'). The stiffness obtained by the average response of nanosprings can be obtained using the contact Hertz law. The resulting Young modulus is estimated at $E_{VANS} = 1.5 \pm 0.1$MPa [5]. These mechanical properties are compared with those of more common particulate coatings.

The latter are formed by the deposition aqueous suspensions of nanoparticles on a glass microscope slide: suspensions of nanosilica spheres whose size is 7nm (Ludox SM30), 12nm (Ludox HS40), and nanoclay platelets whose size is 220nm (purchased from Sigma-Aldrich). The drying under room conditions results in close packing networks of particles. Using indentation testing, the elastic modulus of dried nanosilica films, E_{silica}, is such that [11]:

$$\frac{E_{VANS}}{E_{silica}} \sim 10^{-3} \qquad (1)$$

In the following, the crack patterns induced by drying both nanospring and nanoparticle films are imaged using reflected light microscopy in fig. 1a,b. For image analysis, the contrast between cracks is improved using a standard thresholding method to yield a binary image that comprises only cracks and background.

Crack formation. – When drying a film of particles, the solvent loss leads to a high contraction of the particle assembly. Since the film is free to contract vertically in response to stress, the shrinkage at the free surface is

frustrated by the adhesion to the substrate. The large tensile stresses result in cracks formation [12]. The cracks invade the plane of the film through successive generations so dividing the plane of the film into adjacent fragments (fig. 1b).

In the case of nanospring films, the crack formation is induced by a wetting and drying process as sketched in fig. 2b. Starting from a homogeneous surface, the wetting process consists in depositing a drop of a low-surface-tension and volatile liquid of typically 3μl at the surface of the film (see Supplementary Material 'S2'). The drop spreads and rapidly soaks into the porous film when the local pressure at the surface of the film is overcome by the capillary pressure. This process is well adapted to nanospring films that exhibit high permeability, k [5]. The characteristic time for the imbibition process is deduced from the Darcy law as: $t_{imb} \sim \frac{\mu_s z^2}{k\Delta P_{cap}}$, where μ_s is the viscosity of the liquid, z is height over which soaking occurs (close to the film thickness), $\Delta P_{cap} = \frac{2\gamma_{lv}\cos(\theta)}{R}$ is the pressure difference at the evaporation surface induced by the surface tension of the solvent with air, γ_{lv} (θ is the contact angle of the liquid and the solid film, and R is the radius of curvature of the menisci at the liquid-vapour interface). The drying process naturally starts during the imbibition process and continues after the liquid is entirely imbibed into the layer. The drying timescale is given by $t_D = \frac{h}{V_E}$, where V_E is the evaporation rate of the solvent in the air. Note that the crack pattern are induced by wetting and drying process of ethanol; the same results are obtained with drops of surfactant-containing water since a drop of pure water keeps a spheroidal shape due to the air pockets trapped underneath. Under ambient conditions, $V_E \approx 5.10^{-7} m.s^{-1}$ and $t_D \sim 40s$ (10 times higher in the case of water). In any case $t_D \gg t_{imb}$. The capillary force acting on the nanosprings leads to their collapse (fig.2c). Hence, the nanosprings deflection, δ, is determined by [13]: $\delta = \frac{\Delta P_{cap} h^4 . d}{8\mathcal{E}I}$, where d and h are the diameter and the heigth h of the nanospring, respectively, $\mathcal{E}$ is the nanospring Young modulus, and $I = \pi d^4/64$ is the cross-sectional second moment of a single nanospring assimilated to a wire of diameter d and heigth h, the film thickness. The deflection of the nanosprings results in the aperture of the film that scales as $w \sim 2\delta$ (fig.2c). Considering a film of nanosprings of averaged diameter $d = 10$nm, of length $h = 26\mu$m, and elastic modulus $\mathcal{E} = 0.30 \pm 0.04$TPa, the capillary pressure associated with $R \sim w$ is estimated at $3k$Pa. The resulting deflection is $25 \pm 3\mu$m that is consistent with the crack opening that are measured in the experiments. The crack widening occurs during propagation. At the end of the drying process, the stress release results in the partial crack closure. Indeed, 80% of the crack opening is relieved in the case of nanospring films in comparison with 20% in nanosilica films [5]. This emphasises the high degree of elasticity of nanospring films.

The crack growth induced by the drying and wetting process of nanospring films shows tortuous paths. The resulting network contains some junctions and a large number of dead-end cracks as shown in fig. 1a. The morphology is qualitatively different from that of brittle films (fig. 1b). In addition, analysis based on Graph theory can be used to compare these morphologies quantitatively using relevant indicators [14,15]. One possible way of quantitaively distinguishing between these morphologies is to consider the distribution of crack lengths.

In the sequential formation, the longest cracks, e.g. the 1st rank, are only a few: since they are the first to spread, they do not connect to any existing cracks (fig. 1b). The cracks of rank 2 connect to the first one (or emerge from the first one): they are more numerous. And so on... This results in the distribution of crack lengths measured between two terminations as shown in the plot fig. 1d. Hence, the cracks tend to form a self-similar structure as underlined by the power law in accordance with reference [16].

In the case of patterns exhibiting a low degree of hierarchy as shown in fig. 1a, the determination of crack lengths associated with their rank is more uncertain leading to more inaccuracies in length measurements (fig. 1c). However, the distribution of crack lengths is clearly different from the hierarchical case: the size distribution is spread over a finite range with a density that barely depends on the average length of the cracks. In the following, we focus on the potential evolution of the crack networks reported in fig. 1a&b during repeated stresses of the films.

Evolution of the crack patterns with repeated wetting and drying cycles. – The evolution of a crack pattern is investigated through successive wetting and drying processes of the film initially dry at equilibrium with the surrounding conditions. The study is mainly carried out on the nanospring films, then compared with the case of more classical brittle films.

Progressive crack extension in nanospring films.

In the case of nanospring films, a typical sequence of images show that the crack network evolves with each wetting and drying cycle (fig. 3a). At the final stage of a wetting and drying process, the crack network does not evolve anymore providing that there is insufficient energy to grow the crack path locally. The crack growth is affected by the existing crack network. The nucleation of new cracks takes place at a sufficient distance from existing cracks; however, the endpoints of the open crack network are more frequently the preferential location to extend the crack path. A simple network analysis which is based on the total length of the cracks for a given surface area shows that the overall crack length progressively increases during each cycle (fig. 3b,c). This is highlighted by the vertical dashed lines for various film thicknesses in fig. 3b. Moreover, between two consecutive cycles, the length of the network ceases to propagate which is highlighted by the horizontal dashed lines in fig. 3b,c. Thus, the crack network progressively extends with increasing cycles, following a staircase-like line. This behaviour is strongly dif-

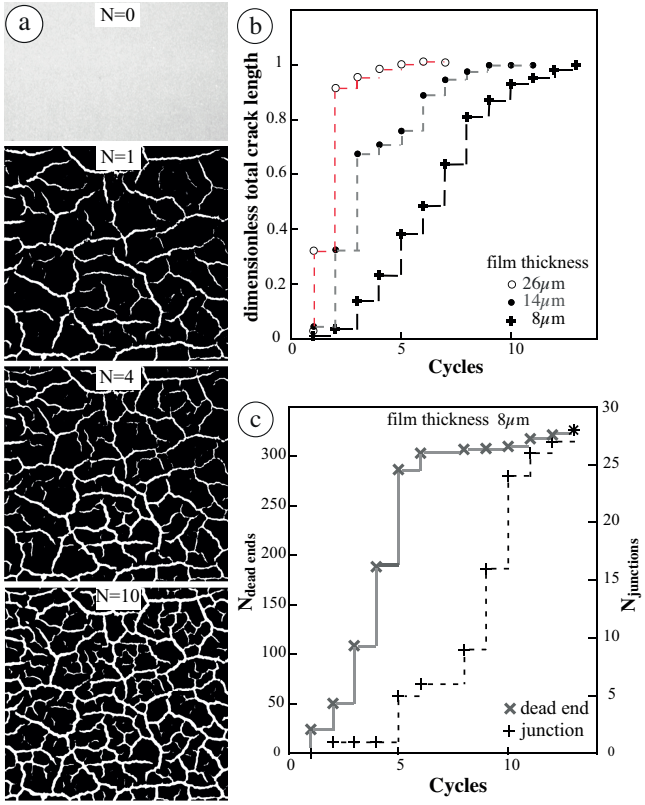

Fig. 3: Evolution of crack networks during successive wetting/drying cycles of nanospring films. (a) Starting from a homogeneous surface (grayscale image), the sequence of images exhibits the crack evolution with subsequent wetting/drying cycles (N refers to the cycle number). Variations of both the total length of cracks for three films thicknesses (b), and the number of dead-end cracks, $N_{dead-ends}$, and crack-junctions, $N_{junction}$, (c) during successive wetting/drying cycles. Measurements are performed on a given surface area three times larger than the images in (a).

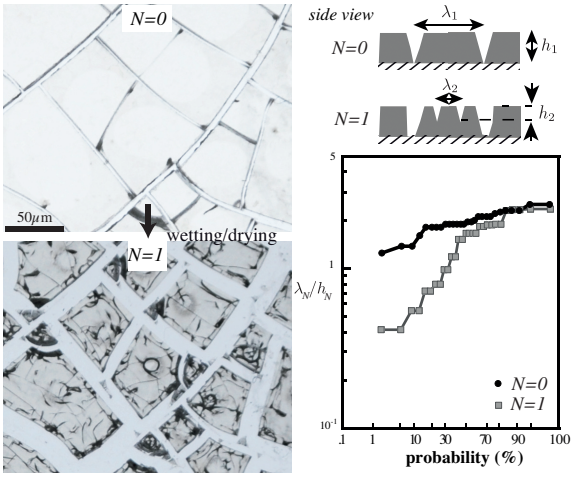

Fig. 4: Image *N=0* exhibits a crack pattern induced by drying of a nanosilica film (HS); The mean crack spacing is λ_1 (dried film thickness: $h_1 = 25\mu$m). Following a wetting and drying process, the crack network evolves as shown in image *N=1*: the existing cracks exhibit a larger aperture while new cracks spaced λ_2 apart do not extend through the whole thickness of the coating (sketch in side view). Plot: correlation between crack spacing, index λ_i, and thickness, h_i, obtained for 3 nanosilica films of thickness 15, 25 and 30μm.

ferent from that of a more classical material, where cracks rapidly invade the plane of the film (fig. 4-$N = 0$). Note that further wetting and the drying of brittle films leads to partial delamination induced by differential shrinkage causing the solid fragments to peel [21]. However, this process is not suitable in the case of nanospring films, due to the synthesis of nanowires themselves. Hence, the delamination process was prevented in brittle films by increasing the adhesion energy of the film on the substrate. Then, the wetting and drying process drives the formation of a pattern of new cracks that do not extend through the whole film thickness as sketched in the side view in fig. 4-$N = 1$. The depth of these new cracks can be estimated through differential focusing under optical microscopy.

One of the main differences in the evolution of the crack networks is related to the film's ability to propagate a crack. In nanospring films, the crack widens during its propagation with a timescale t_D. Contrastingly, classical films suddenly fail; in drying films the propagate timescale is very short compared with the drying timescale. This is mainly due to film stiffness. Usually, the highest crack velocities are at least an order of magnitude smaller than the elastic shear wave velocity for an incompressible material, $\sqrt{E/\rho}$, where E is the elastic modulus of the film and ρ its density. In particular, considering equation 1, the ratio of the highest propagation speed in nanosilica films is 30 times higher than that in nanospring films.

Stabilization of the crack network over successive stresses.

The change in the network topology over wetting and drying cycles is described by the evolution of the number of junctions and dead-end cracks as reported in fig. 3c. Surprisingly the crack network presents still a low connectivity since it contains scarcely any junctions cracks. This applies to different thicknesses (see Supplementary Materials S3). The number of dead-ends significantly increases with repeated cycles despite the progressive coalescence of some cracks. This is mainly due to crack growth that emanates from kink points of the existing network. After around ten wetting and drying cycles, the crack network reaches stabilization when the cracks stop growing. Consequently, the more cycles the film undergoes, the more equilibrated the cracking degree will be. A physical mechanism responsible for this stabilization follows.

(i) In the first case, a crack connects to another crack, so eventually forms a junction. Indeed, when a crack is formed, the component of the stress normal to the crack path is released on a lengthscale that is proportional to the film thickness [18]. Then, when a future crack approaches the former one, its path is changed due to the stress release of the first one. The new crack connects to

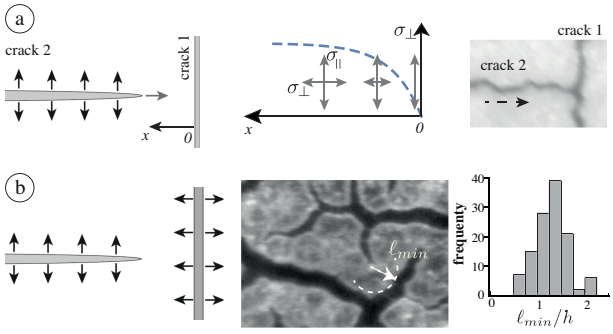

Fig. 5: (a) Hierarchical formation of cracks. Stress components, $\sigma_\parallel$, $\sigma_\perp$ are parallel and perpendicular to the surfaces of crack 1, respectively. After the formation of crack 1, $\sigma_\perp$ is released in the vicinity of the crack surfaces, over a lengthscale captured by the dashed curve in the plot. Then, when approaching crack 1, crack 2 path is guided by the modified stress components. This results in a crack-junction. (b) Simultaneous formation of cracks. Crack tip arrest when approaching a neighboring crack that still opens. This results in a dead-end crack. The separating distance between the crack tip and the neighboring crack reaches a minimum value, ℓ_{min}. Statistics on ℓ_{min} follows a Normal distribution.

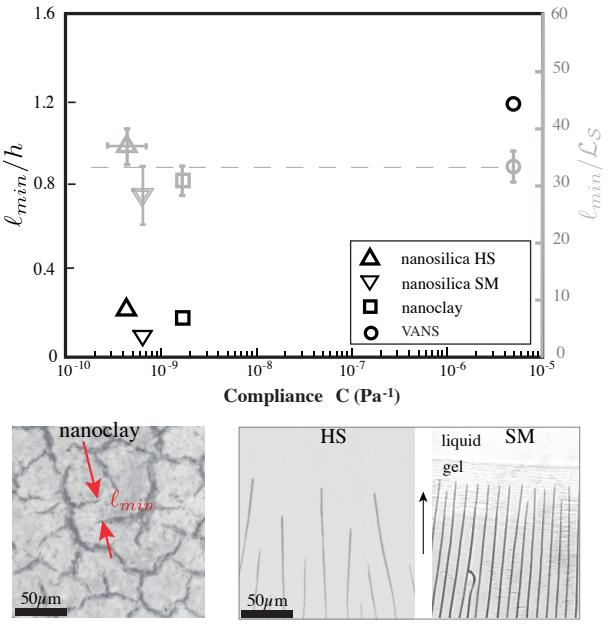

Fig. 6: Plot on semi-log scale showing the minimum separation distance, ℓ_{min}, between a crack tip and the nearest neighbouring crack as a function of the film compliance, $C = E^{-1}$: ℓ_{min} is normalized to the film thickness, h (black dots, left vertical axis), and to the shield lenghtscale, $\mathcal{L}_S$ (grey dots, right vertical axis). Each dot corresponds to a statistic on about 10 dried films. The components of the films are described in the Table 1. Uniform drying results in isotropic crack networks whereas directional drying induced by a thickness gradient results in a directional growth of cracks (framed images for HS and SM). The dashed line is a guide for the eyes.

its neighbour perpendicularly. This process is encountered in brittle films and less frequently in systems with a lower degree of hierarchy.

(ii) In the second case, cracks form simultaneously. In other words, cracks are formed much faster than they grow. Let us consider a crack tip approaching the surface of a neighbouring crack that still opens as illustrated in fig. 5b. Since the stress release from the crack surface is not triggered yet, the part of the film separating the crack tip is in compression and does not allow the crack connection. This results in a termination crack involving a separation distance between a crack tip and the neighbouring cracks. This local pattern does not evolve under repeated stress in the condition of simultaneous opening of cracks.

Open networks of cracks with dead-end cracks are observed nanospring films and more generally when crack propagation is energetically unfavourable: this is the case for materials with low elastic energy because due to compliance or in thin films where the elastic energy is weakly stored. This is particularly the case for thin films of nanosilica particles or nanoclay as described in Table 1. Thus, the shortest separation distance, ℓ_{min}, at which the crack no longer propagates was measured for different coatings, each of them exhibiting specific mechanical properties: thin brittle nanosilica films resulting from the drying of various nanoparticles suspensions (SM & HS), softer film of nanoclay, and compliant nanosprings (graph in fig. 6). These measurements were extended to the case of directional crack growth induced by a thickness gradient [19]. Usually a network of parallel cracks form, the crack tips propagate following a drying front. In some particular events a crack tip propagates with a small delay compared to the others: then the crack tip stops growing (image HS in fig. 6). However, if the delay is significant, the crack stops growing it connects perpendicularly to one of the neighbouring crack (image SM in fig. 6).

Thus, the distance ℓ_{min} appears to be affected by the ability of the material to deform, which can be quantified through the compliance $C = E^{-1}$.

In addition, closely interacting cracks typically provide a "shielding zone" which tends to reduce the stresses between adjacent cracks [20]. The resulting confinement can be captured by the lengthscale, $\mathcal{L}_S$, that is pointed out by a simple energy balance:

$$\mathcal{L}_S = W/E\epsilon^2 \qquad (2)$$

where W is the bonding energy of the material, E its elastic modulus, and ϵ the strain induced by the drying process. This last is estimated as: $\epsilon = w_m/h$, where w_m is the maximum crack opening. The bonding energy, W, is estimated to be 1 mJ/m^2 for the different films of nanoparticles from reference [20] and 1.7 mJ/m^2 for the nanosprings [10]; the elastic modulus, E, is estimated through microindentation performed on dried nanoparticle films [11] for

Table 1: List of elementary components of dry films: their size, the compliance resulting from the measurements of the elastic modulus using indentation testing, and the characteristic of the isotropic crack network that no longer evolves with repeated wetting and drying cycles. ∘ corresponds to open network of cracks while • corresponds to closed networks of cracks.

film component	Compliance $\times 10^{-9} Pa^{-1}$	thickness $8 \pm 3\mu$m	thickness $20 \pm 3\mu$m
silica HS-12nm	0.4	∘	•
silica SM-7nm	0.8	∘	•
clay-220nm	1.8	∘	∘
VANS	5.10^3	∘	∘

wet nanosprings; the strain, ϵ, is estimated from the maximum value of the crack aperture over the film thickness. Hence, using the experimental measurements reported in fig. 6, the dimensionless quantity $\ell_{min}/\mathcal{L}_S$ appears to be of the same order of magnitude for stiff and compliant films (fig. 6). This highlights the shielding effect resulting from interacting cracks.

Conclusion. – We investigate the formation of drying cracks in nanostructured films consisting of vertically aligned helical nanowires. Over repeated wetting and drying cycles a crack network forms and evolves intermittently. The analysis shows that the cracks are progressively confined through their mutual interaction leading to either connecting to a neighbouring crack or ends at a separation distance. The stabilization of the crack network is determined by shield effect that points out a lengthscale quantified in various coatings, from stiff to compliant, with a range of elastic moduli over four orders of magnitude. The crack patterns are compared to the hierarchical formation of cracks in more classical materials.

* * *

The authors thank Prof. Matteo Ciccotti from ESPCI-Paris for fruitful discussions.

REFERENCES

[1] Wang, C., Zhan-Zhang, Liu, Y. & Shi-Fan Geometric and fractal analysis of dynamic cracking patterns subjected to wetting-drying cycles. *Soil And Tillage Research.* **170** pp. 1-13 (2017)

[2] Giorgiutti-Dauphine, F. & Pauchard, L. Painting cracks: A way to investigate the pictorial matter. *Journal Of Applied Physics.* **120**, 065107 (2016)

[3] Sadhukhan, S., Kumar, A., Kulkarni, G., Tarafdar, S. & Dutta, T. A spring network simulation in three dimensions for designing optimal crack pattern template to fabricate transparent conducting electrodes. *Bulletin Of Materials Science.* **42**, 197 (2019)

[4] Timalsina, Y., Oriero, D., Cantrell, T., Prakash, T., Branen, J., Aston, D., Noren, K., Nagler, J., Rastogi, S., McIlroy, D. & Corti, G. Characterization of a vertically aligned silica nanospring-based sensor by alternating current impedance spectroscopy. *Journal Of Micromechanics And Microengineering.* **20**, 095005 (2010)

[5] Pauchard, L., Giorgiutti-Dauphine, F. & McIlroy, D. Crack quasi-healing in films of vertically aligned 1D nanostructures: Impact of compliance in a 1D geometry. *Journal Of Applied Physics.* **131**, 164701 (2022)

[6] Hafver, A., Jettestuen, E., Kobchenko, M., Dysthe, D., Meakin, P. & Malthe-Sorenssen, A. Classification of fracture patterns by heterogeneity and topology. *Europhysics Letters.* **105**, 56004 (2014)

[7] Bohn, S., Pauchard, L. & Couder, Y. Hierarchical crack pattern as formed by successive domain divisions.. *Phys. Rev. E.* **71**, 046214 (2005)

[8] McIlroy, D., Alkhateeb, A., Zhang, D., Aston, D., Marcy, A. & Norton, M. Nanospring formation - Unexpected catalyst mediated growth. *J. Phys. Condens. Matter.* **16** pp. R415 - R440 (2004)

[9] McIlroy, D., Zhang, D., Kranov, Y. & Norton, M. Nanosprings. *Applied Physics Letters.* **79**, 1540-1542 (2001)

[10] Wojcik, P., Bastatas, L., Rajabi, N., Bakharev, P. & McIlroy, D. The effects of sub-bandgap transitions and the defect density of states on the photocurrent response of a single ZnO-coated silica nanospring. *Nanotechnology.* **32**, 035202 (2020)

[11] Sibrant, A. & Pauchard, L. Effect of the particle interactions on the structuration and mechanical strength of particulate materials. *Europhysics Letters.* **116**, 49002 (2017)

[12] Lazarus, V. & Pauchard, L. From craquelures to spiral crack patterns: influence of layer thickness on the crack patterns induced by desiccation. *Soft Matter.* **7**, 2552-2559 (2011)

[13] Wirth, C., Hofmann, S. & Robertson, J. Surface properties of vertically aligned carbon nanotube arrays. *Diamond And Related Materials.* **17**, 1518-1524 (2008)

[14] Perna, A., Kuntz, P. & Douady, S. Characterisation of spatial network-like patterns from junctions' geometry. *Phys. Rev. E.* **83**, 066106 (2011)

[15] Jeammet, S. (2023). Ruptures Enlacées - Morphogénèse de Reseaux dans l'argile [Doctoral dissertation, University Paris Cité].

[16] Colina, H. & Roux, S. Experimental model of cracking induced by drying shrinkage. *Eur. Phys. J. E.* **1**, 189-194 (2000)

[17] Xia, Z. & Hutchinson, J. Crack patterns in thin films. *Journal Of The Mechanics And Physics Of Solids.* **48**, 1107-1131 (2000)

[18] Beuth, J. Cracking of thin bonded films in residual tension. *International Journal Of Solids And Structures.* **29**, 1657-1675 (1992)

[19] Lee, W. & Routh, A. Why do drying films crack?. *Langmuir.* **20**, 9885-9888 (2004,11)

[20] Lawn, B. Fracture of Brittle Solids. (Cambridge University Press,1993)

[21] Pauchard, L. Patterns caused by buckle-driven delamination in desiccated colloidal gels. *Europhysics Letters.* **74**, 188 (2006)